11-2003

Redshift-Distance Survey of Early-Type Galaxies: Spectroscopic Data

G. Wegner
Dartmouth College

M. Bernardi
Carnegie Mellon University

C. N. A. Willmer
University of California, Santa Cruz

L. N. da Costa
Valongo Observatory

The Astronomical Journal, 126:2268–2280, 2003 November

REDSHIFT-DISTANCE SURVEY OF EARLY-TYPE GALAXIES: SPECTROSCOPIC DATA

G. Wegner,[1] M. Bernardi,[2] C. N. A. Willmer,[3,4,5] L. N. da Costa,[4,5,6] M. V. Alonso,[7,8]
P. S. Pellegrini,[4,5] M. A. G. Maia,[4,5] O. L. Chaves,[5] and C. Rité[4,5,6]

Received 2003 April 29; accepted 2003 August 8

ABSTRACT

We present central velocity dispersions and Mg_2 line indices for an all-sky sample of ~1178 elliptical and S0 galaxies, of which 984 had no previous measures. This sample contains the largest set of homogeneous spectroscopic data for a uniform sample of elliptical galaxies in the nearby universe. These galaxies were observed as part of the ENEAR project, designed to study the peculiar motions and internal properties of the local early-type galaxies. Using 523 repeated observations of 317 galaxies obtained during different runs, the data are brought to a common zero point. These multiple observations, taken during the many runs and different instrumental setups employed for this project, are used to derive statistical corrections to the data and are found to be relatively small, typically $\lesssim 5\%$ of the velocity dispersion and 0.01 mag in the Mg_2 line strength. Typical errors are about 8% in velocity dispersion and 0.01 mag in Mg_2, in good agreement with values published elsewhere.

Key words: galaxies: distances and redshifts — galaxies: elliptical and lenticular, cD — galaxies: general — large-scale structure of universe — surveys — techniques: spectroscopic

On-line material: machine-readable tables

1. INTRODUCTION

If large-scale structures in the universe develop through the action of gravity, their growth induces peculiar velocities that are detectable as deviations of the galaxies' motion relative to the smooth Hubble flow. Therefore, by measuring redshifts and redshift-independent distances for a large number of galaxies, it is possible to map the peculiar velocity field and to use it to probe the characteristics of the underlying mass distribution, as well as to constrain cosmological parameters, by comparing predicted and measured peculiar velocities (e.g., Bertschinger et al. 1990; Strauss & Willick 1995; Nusser & Davis 1994; Willick & Strauss 1998).

Following pioneering attempts (e.g., Rubin et al. 1976; Tonry & Davis 1981; Aaronson et al. 1982) the first successful measurement of peculiar motions in the local universe was carried out by the "Seven Samurai" (7S) group, who developed the D_n-σ distance method for elliptical galaxies and showed in a series of papers (Dressler et al. 1987; Davies et al. 1987; Burstein et al. 1987; Lynden-Bell et al. 1988, Faber et al. 1989) that the mass distribution in the local volume presents significant velocity and mass density fluctuations. The 7S sample is an all-sky survey of about 400 early-type galaxies, generally brighter than $m_B = 13.5$ mag. Analysis of the measured velocity field led to the discovery of the Great Attractor (GA), earlier conjectured by Tammann & Sandage (1985) and later shown to correspond to a large concentration of galaxies in redshift space (da Costa et al. 1986, 1987; Burstein, Faber, & Dressler 1990; Woudt, Kraan-Korteweg, & Fairall 1999).

These surprising results led to the demise of the standard high-bias cold dark matter model, and questions raised by the 7S work motivated attempts to expand the samples of galaxies with measured distances, most of which used Tully-Fisher (TF) distances to spirals (Willick 1990; Courteau et al. 1993). However, most of these more recent investigations either had limited sky coverage or used very sparse samples. Major progress only became possible after the completion of wide-angle redshift-distance TF surveys, such as those conducted by Mathewson, Ford, & Buchhorn (1992) and Mathewson & Ford (1996) and the SFI survey (e.g., Haynes et al. 1999a, 1999b) of spiral galaxies. These new surveys have been assembled to produce homogeneous all-sky catalogs, such as the Mark III (Willick et al. 1997), the SFI catalog (e.g., da Costa et al. 1996; Giovanelli et al. 1998), and SHELLFLOW (Courteau et al. 2000). These data have been extensively used in recent analyses, but, despite the qualitative similarity of the recovered flow fields, a quantitative comparison shows conflicting results, illustrated by different estimates of the parameter $\beta = \Omega^{0.6}/b$, where Ω is the cosmological density parameter and b is the linear bias factor relating galaxy and mass density fluctuations (e.g., da Costa et al. 1998a; Zaroubi et al. 1997; Willick & Strauss 1998). Using the POTENT density-density method tends to produce higher values of β than does the VELMOD velocity-velocity technique, although more recent results are more consistent (Zaroubi et al. 2002).

Recent work on the motions of early-type galaxies, such as Lauer & Postman (1994), Müller et al. (1998, 1999), the

[1] Department of Physics and Astronomy, Dartmouth College, 6127 Wilder Laboratory, Hanover, NH 03755.
[2] Department of Physics, Carnegie Mellon University, Pittsburgh, PA 15213.
[3] UCO/Lick Observatory, University of California, Santa Cruz, 1156 High Street, Santa Cruz, CA 95064.
[4] Observatório do Valongo, Ladeira do Pedro Antonio 43, 20080-090 Rio de Janeiro, RJ, Brazil.
[5] Observatório Nacional, Rua General José Cristino 77, 20921-400 Rio de Janeiro, RJ, Brazil.
[6] European Southern Observatory, Karl-Schwarzschild-Strasse 2, D-85748 Garching, Germany.
[7] Observatorio Astrónomico de Córdoba, Laprida 854, 5000 Córdoba, Argentina; and CONICET.
[8] Laboratoire d'Astrophysique, Observatoire Midi-Pyrénées, 14 Avenue Edouard Belin, F-31400 Toulouse, France.

EFAR survey (Wegner et al. 1996; Colless et al. 2001), and SMAC (Hudson et al. 1999), were designed to extend our knowledge of the peculiar motions of galaxies to greater distances ($R \sim 60\ h^{-1}$–$110\ h^{-1}$ Mpc, where $h \equiv H_0/100$ km s^{-1} Mpc^{-1}) in sparser surveys, some of which only cover part of the sky. For most of these investigations, the fundamental plane (FP) method was employed. More recent distance methods, such as Type Ia supernovae (Riess 2000) and surface brightness fluctuations (Tonry et al. 2000), are more accurate than the methods related to TF or FP on a per object basis, e.g., $\Delta R/R \sim 5\%$–7% compared with $\sim 20\%$–25% for D_n-σ, but have neither the numbers of objects nor the depth ($R \sim 50\ h^{-1}$ and $30\ h^{-1}$ Mpc, respectively) to reconstruct the velocity flows (see Dekel 2000 and Colless et al. 2001 for compilations of recent peculiar motion surveys and their depths). Thus a new all-sky survey of early-type galaxies extending the earlier 7S sample has been needed.

Such an all-sky survey has been the goal of the Redshift-Distance Survey of Nearby Early-Type Galaxies (ENEAR). The sky coverage and selection of the survey have been given in da Costa et al. (2000a, Paper I). It is an all-sky redshift-distance survey of early-type galaxies, within $cz \leq 7000$ km s^{-1}, drawn from an $m_B = 14.5$ magnitude-limited sample with complete redshift data. The completeness and selection criteria of the ENEAR sample have been detailed in Paper I and given in Figure 10 of that paper, which also provides maps of sky coverage and other information on the survey, and, in general, the sample completeness is nearly constant, at $\geq 80\%$ for the above magnitude and redshift limits. During the course of the ENEAR project, it was necessary to add cluster galaxies outside these criteria that were used to calibrate the D_n-σ relation. These objects are more distant and fainter than the criteria above used for the ENEAR selection and have been described in Bernardi et al. (2002a, 2002b). Further galaxies were also observed to compare our data with the literature.

With nearly 3 times the number of galaxies and a fainter limiting magnitude, the ENEAR survey has greater depth ($R \sim 60\ h^{-1}$ Mpc) and resolution than the 7S study ($R \sim 30\ h^{-1}$ Mpc), and it is intended to complement the SFI spiral TF ($R \sim 65\ h^{-1}$ Mpc) survey, with comparable depth and sky coverage but employing different distance relations. Using early-type galaxies, one hopes to settle some of the pending issues. These include testing the universality of the results from the SFI and related flow studies based on spiral galaxies using a completely independent sample, based on a different distance relation and a galaxy population that closely follows the ridges of structures, in contrast to the more widely distributed spiral population.

A number of analyses have already been carried out using ENEAR data, and they indicate that the cosmic flows found from the early-type and spiral galaxies are indeed statistically equivalent. Borgani et al. (2000) studied the velocity correlation function of the ENEAR clusters and found they agree well with the SCI spiral cluster sample. Da Costa et al. (2000b) found that the dipoles defined by the flow of the ENEAR early-type galaxies agree well with that of the SFI spirals using TF distance measurements. Nusser et al. (2001) compared ENEAR and *IRAS* PSCz velocity fields and obtained good agreement between the early-type and spiral galaxy results. Zaroubi et al. (2001) studied the large-scale power spectrum of the ENEAR velocity field and derived the density field, finding that most of the Local Group's motion is produced by mass fluctuations within 80 h^{-1} Mpc. Feldman et al. (2003) combined ENEAR data with other surveys to derive Ω_m and σ_8. Bernardi et al. (1998) studied the Mg_2 line strengths of ENEAR galaxies in three different density regimes, ranging from high to low, finding that their galactic spheroids must have formed at redshifts ($z \gtrsim 3$) independently of their present environments. Bernardi et al. (2002a, 2002b) described the construction of the D_n-σ template from early-type galaxies in clusters that have been used to estimate distances and derive peculiar velocities.

Here we present the spectroscopic data of the ENEAR survey, which complement the photometric data presented by Alonso et al. (2003). This paper is organized as follows: § 2 presents a brief description of the sample, as well as the observations and reduction procedures used for the spectroscopic data. Section 3 presents the techniques used to measure redshifts, velocity dispersions and Mg_2 indices; in this section we also discuss the calculation of the internal errors, and the corrections applied to the data due to observational effects. In § 4 we describe the procedure that was used to create the master catalog of homogeneous measurements with their estimated errors. In § 5 we present the calibrated and fully corrected measurements. A brief summary follows in § 6.

2. THE SPECTROSCOPIC DATA

2.1. *The Sample*

Here we present spectroscopic parameters for 1178 galaxies from measurements obtained from 1701 spectra. We have collected data for a sample of early-type galaxies ($T \leq -2$ in the Lauberts & Valentjin 1989 system), which combines galaxies from: (1) the ENEARm sample consisting of galaxies brighter than $m_B \leq 14.5$ within 7000 km s^{-1} (Paper I); (2) our measurements for galaxies in cluster/groups in the ENEARc sample used by Bernardi et al. (2002a, 2002b) that adhere to these same two selection criteria; (3) galaxies in the SSRS2 (da Costa et al. 1998b) with an adequate signal-to-noise ratio (S/N) to reliably measure the velocity dispersion and line indices. Paper I and Bernardi et al. (2002a) also describe the ENEAR sample and subsamples. Figure 1 gives a histogram of the morphological types for the galaxies in this paper.

2.2. *Observations*

The spectroscopic observations reported here were made over several years from three sites (CASLEO[9], ESO[10], and MDM[11]). During our program 30 spectroscopic observing runs were carried out at the different sites. In total, there were 127 usable nights for spectroscopic observations in the period 1992–1999. Eleven setups were employed corresponding to different combinations of telescope, detector, and spectrograph, and the resolution varied from about 2 to 5 Å. A total of 1701 spectra were obtained. Table 1 summarizes the observations listing: in column (1) the run identification number; in column (2) the date of the observations; in column (3) N_s the number of spectroscopic nights for the

[9] Complejo Astronomico El Leoncito (Argentina).
[10] European Southern Observatory (Chile).
[11] MDM Observatory (Arizona).

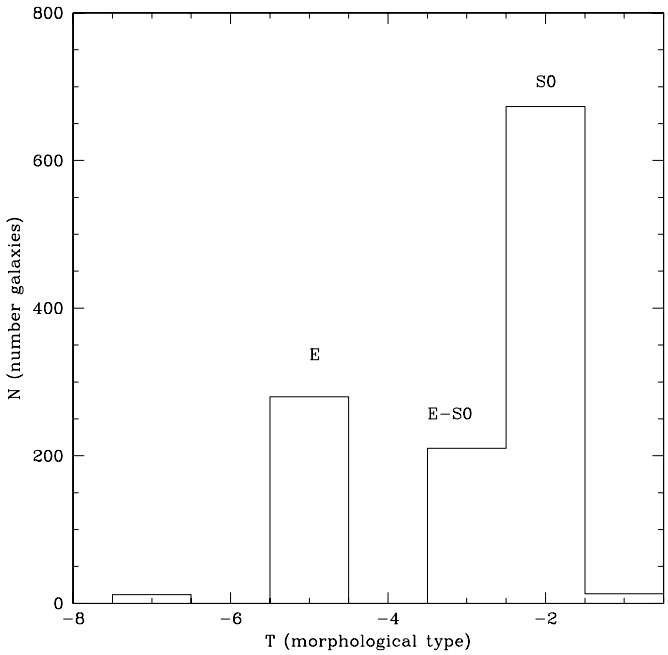

FIG. 1.—Distribution of morphological T types on the system of Lauberts & Valentijn (1989) for the galaxies in this paper. Approximate Hubble types are also given above each of the columns.

TABLE 1
OBSERVING RUNS FOR SPECTROSCOPY

Run (1)	Date (2)	N_s (3)	Setup (4)
MDM-501	1992 Oct	5	5
ESO-651	1993 Nov	6	1
ESO-652	1994 May	7	1
MDM-502	1994 Oct	6	6
ESO-654	1995 May	1	2
ESO-653	1995 Aug	4	1
MDM-503	1995 Dec	4	7
CASLEO-801	1996 Apr	3	11
CASLEO-802	1996 Sep	3	11
ESO-655	1996 Oct	5	4
ESO-656	1996 Nov	13	3
MDM-505	1996 Nov	3	8
ESO-657	1997 Jan	5	3
MDM-506	1997 Feb	2	9
ESO-658	1997 Mar	6	4
ESO-659	1997 Apr	10	4
CASLEO-803	1997 May	5	11
MDM-507	1997 Jun	5	10
ESO-660	1997 Oct	5	4
MDM-508	1997 Nov	3	9
ESO-661	1998 Feb	6	4
ESO-662	1998 Apr	7	4
MDM-509	1998 Apr/May	2	9
ESO-663	1998 Jun	3	4
ESO-664	1998 Aug	2	4
ESO-665	1998 Oct	4	4
MDM-510	1998 Nov	1	9
ESO-666	1999 Feb	11	4
ESO-667	1999 Aug	2	4

NOTES.—Col. (3) shows the number of spectroscopic nights for the run. Information about the setup indicated in col. (4) is given in Table 2.

run, and in column (4) the setup reference number described below.

Table 2 summarizes the different setups: in column (1) the setup reference number; in column (2) the observatory and telescope used; in columns (3) and (4) the number of spectra N_m, and the number N_r of repeated observations using each setup; in columns (5)–(9) the characteristics of the detector, such as its identification, size, pixel scale, gain, and readout noise; in columns (10)–(13) the characteristics of the spectrograph, such as the slit width, the grating, the dispersion, the resolution (as measured from the width of the calibration lines), and the spectral coverage. All new spectra were obtained using long slits. The resolutions used can be divided into two groups, which we refer to as the high (~2.5 Å) and low resolution (~5 Å), the low-resolution setups being 2, 3, 6, 7, and 10. Note that ~80% of the spectra were obtained at high resolution.

As the goal of the new spectroscopic observations was to measure both central velocity dispersions and line strengths, the spectral range was chosen to cover the Mg b band (around $\lambda_0 = 5177$ Å), the E band (5270 Å), and the Fe I line (5335 Å). Most of our observations also included Hβ (4861 Å).

We followed standard procedures for observing the CCD spectra. In general, identical observational and reduction procedures were used for ESO and CASLEO data. Wavelength calibration lamps were observed before and after each object (He-Ar at ESO; Hg-Ar-Xe-Ne at MDM; He-Ne-Ar at CASLEO). Dome flats, bias, and dark current frames were taken nightly. The dark current was checked for each CCD, but always found to be negligible. Usually, multiple exposures of a given galaxy were taken to facilitate cosmic-ray removal. Exposure times varied with object and sky conditions, but typical values were 10–20 minutes at MDM and 20–30 minutes at ESO and CASLEO.

During each night stars with known radial velocities in the spectral range of G8 to K5 and luminosity class III were observed for use as velocity templates. The MDM spectra were trailed along the slit and the ESO data consisted of single exposures along the slit. We also observed a subset of the Lick standards (Worthey et al. 1994) covering a wide range of spectral types. Normally velocity standards were observed nightly, and several were observed during each observing run.

Determining velocity dispersions requires relatively high-S/N spectra compared with that needed for redshifts alone. Consequently, for the galaxies we endeavored to obtain around 600 photons Å^{-1}, which corresponds to S/N ~ 25, in continuum bands near the Mg_2 features used for determining both σ and the Mg_2 index. The quality of each observed spectrum was estimated from the mean of the S/N ratios measured at the continuum bands 4895–4957 Å and 5301–5366 Å, in the vicinity of the spectral region where the Mg_2 index is computed. The resulting distribution of S/N for our sample in the Mg_2 region is shown in Figure 2. The median S/N of our spectra is 26.8, slightly above our goal, with a rms scatter of 9.5, but with a large tail extending to higher S/N.

Some of the brighter program galaxies were chosen as standards, and they were systematically observed at least once every run when favorably placed on the sky. This subsample contains ~200 galaxies that were observed twice or more, and the number of repeated observations range from two to 12 for a given galaxy. These measurements were used

TABLE 2

OBSERVING SETUPS

Setup (1)	Telescope (2)	N_m (3)	N_r (4)	Detector (5)	Size (6)	Spatial Scale (arcsec pixel^{-1}) (7)	Gain (e^- ADU^{-1}) (8)	Readout Noise (e^-) (9)	Slit Width (arcsec) (10)	Grating (line mm^{-1}) (11)	Dispersion (Å pixel^{-1}) (12)	Cover Resolution (Å) (13)	Spectral Range (Å) (14)
1.....	ESO 1.52	237	65	CCD No. 24	2048 × 2048	0.72	2.9	8	2.5	600	0.93	2.33	4500–6300
2.....	ESO 1.52	4	-	CCD No. 24	2048 × 2048	0.72	2.9	8	2.5	600	1.87	4.68	3750–7300
3.....	ESO 1.52	114	10	CCD No. 39	2048 × 2048	0.72	1.2	5.5	2.3	600	1.91	4.97	3750–7300
4.....	ESO 1.52	831	218	CCD No. 39	2048 × 2048	0.72	1.2	5.5	2.5	1200	0.98	1.90	4300–6200
	...	1186	293	...	...	...	...	...	...	...	...	...	...
5.....	MDM 2.4	30	6	Willbur	2048 × 2048	0.172	1.94	4.73	1.7	600	0.99	2.00	5180–7200
6.....	MDM 2.4	47	4	Willbur	1024 × 1024	0.343	2.43	4.73	1.7	600	2.81	5.60	4200–7000
7.....	MDM 2.4	56	7	Charlotte	1024 × 1024	0.28	3.16	5.45	1.7	600	2.24	4.48	4500–6800
8.....	MDM 2.4	53	4	Templeton	1024 × 1024	0.28	3.47	5.33	1.7	1200	1.00	2.50	4800–5800
9.....	MDM 2.4	173	48	Charlotte	1024 × 1024	0.28	3.16	5.45	1.7	1200	1.00	2.50	4800–5800
10.....	MDM 1.3	50	4	Charlotte	1024 × 1024	0.51	3.16	5.45	1.2	600	2.10	4.50	4358–6882
	...	409	73	...	...	...	...	...	...	...	...	...	...
11.....	CASLEO 2.15	106	13	Tek	1024 × 1024	...	1.98	7.4	3	600	1.62	3.41	4500–6100
	...	106	13	...	...	...	...	...	...	...	...	...	...
Total.....	...	1701	379	...	...	...	...	...	...	...	...	...	...

NOTES.—Run 6 used 2 × 2 pixel binning. Runs 5, 6, 7, and 10 used the Mark III spectrograph. Runs 8 and 9 used the Modspec spectrograph.

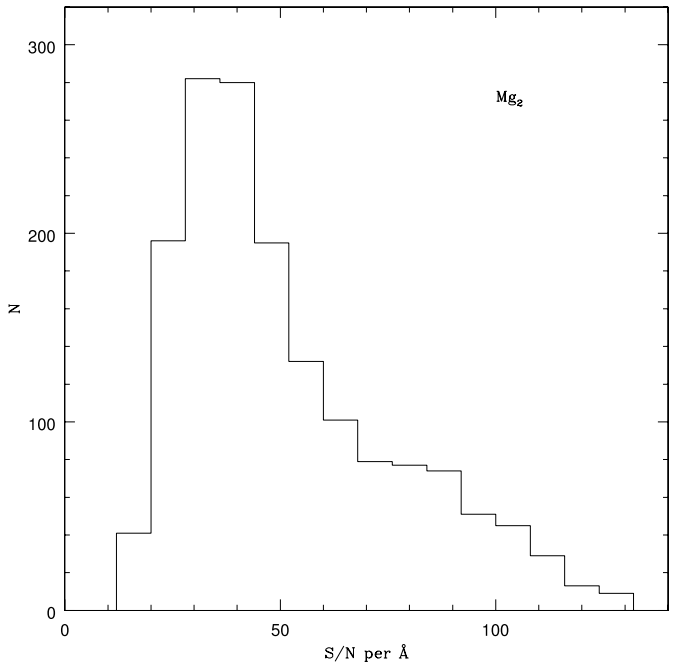

FIG. 2.—Distribution of the S/N per angstrom of the ENEAR spectra in the region of the Mg_2 feature.

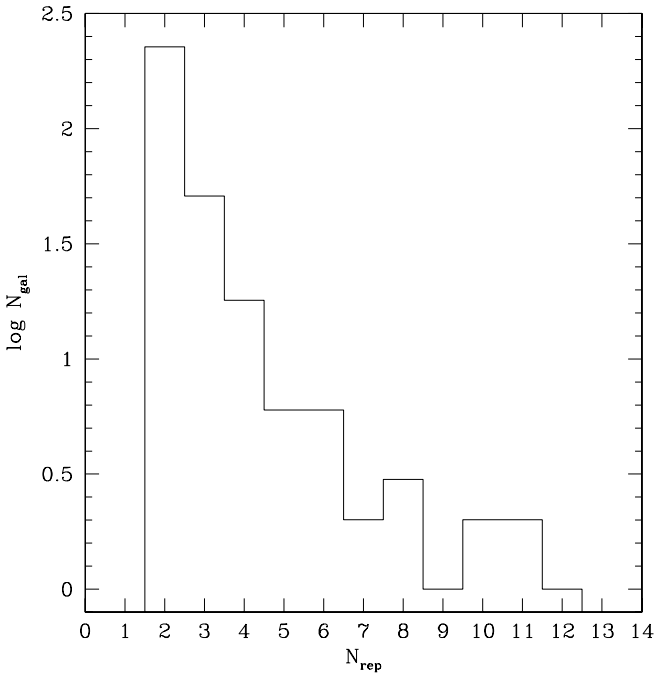

FIG. 3.—Distribution of the internal repeated observations

to compare the low- with high-resolution spectra and to place measurements obtained with different setups and telescopes on a uniform internally consistent system. Figure 3 shows the distribution of repeated observations.

2.3. *Data Reduction*

All spectra were reduced using the standard long-slit procedures in the IRAF[12] package. The reductions are described briefly herein and follow standard methods (e.g., Wegner et al. 1999, where further details can be found) using the following steps: bias subtraction; flat field correction; rejection of the cosmic-ray hits; wavelength calibration; subtraction of the sky spectrum; and extraction of the one-dimensional spectra. All but the last step was done on the two-dimensional images, which provides line rectification. Each run was reduced by one person and, even though similar, the reductions of the MDM and ESO/CASLEO data were done independently with minor procedural differences, pointed out below.

Nightly sets of bias frames were scaled by the level of the CCD overscan strip and medianed. These were checked for temporal variations, and then the resulting bias frame was subtracted from the other images to remove the bias structure. Because of the stability of the systems at ESO, CASLEO, and MDM, median bias frames could be constructed for the entire run and then subtracted from the remaining frames.

Pixel-to-pixel sensitivity variations were removed by median-filtering the flat-field exposures, typically 10 or more per night. These were usually produced from exposures of tungsten lamps either inside the spectrograph, as at MDM, or an illuminated target inside the dome at ESO and CASLEO, passing through the optics of the spectrograph. A map was produced by normalizing the flat field constructed from the combined spectra relative to a smoothed version of itself. The rms variation in the resulting flattened response frames was typically less than 0.5%. Each galaxy or star spectral frame was then divided by this response function map.

Cosmic-ray hits were removed as follows. For MDM and most of the ESO spectra the IRAF LINECLEAN routine was employed. This fits the galaxy's spectrum along the direction of the dispersion and identifies cosmic-ray hits without affecting the absorption lines. For CASLEO and some ESO spectra IMEDIT was used to remove the cosmic-ray hits.

Wavelength calibrations were produced by fitting a polynomial, typically fifth-order, to the comparison spectra, with a fitting accuracy of about ± 0.1 pixel. The wavelength calibrations generally employed more than 20 lines and produced residuals of order ± 0.02 Å for the ESO 1200 line mm^{-1} grating spectra, which is representative for our observations. The wavelength calibration for ESO spectra used the set of He-Ar lines compiled by M. P. Diaz.[13] These gave consistently better solutions than the standard tables distributed with IRAF.

Sky subtraction was facilitated using the sky level determined in the IRAF BACKGROUND routine from two or more regions on each side of the galaxy spectrum far enough not to be contaminated by the object itself. The sky level at the object was interpolated using a low-order polynomial fitted to the sky in a direction perpendicular to the spectrum.

Each final one-dimensional galaxy spectrum was then extracted by summing across its profile on the CCD image

[12] IRAF is distributed by the National Optical Astronomy Observatories which is operated by the Association of Universities for Research in Astronomy, Inc., under contract with the National Science Foundation.

[13] Available from ftp://www.lna.br/instrum/cass/hearlna.dat.Z.

in the region where it was greater than about 5% of its maximum using the IRAF task APSUM with the variance weighting option. For some of the ESO observations the object spectra were extracted by summing the region where the galaxy flux approaches the sky level and the sky value was determined from the median value measured in two regions on each side of the galaxy and then interpolated across the galaxy spectrum.

Finally, all one-dimensional spectra were visually inspected. About 10% of the observed galaxies show some emission lines characteristic of H II regions, while others exhibit features typical of A and F stars (hydrogen Balmer-line absorption). These cases are listed in the comments to Table 4.

3. SPECTROSCOPIC PARAMETERS

3.1. *Redshifts and Velocity Dispersions*

The measurements of the redshift, cz, and the velocity dispersion, σ, were obtained using the IRAF task FXCOR in the *RV* package. This task employs the Tonry & Davis (1979) cross-correlation technique which generally yields more robust measures for modest S/N spectra than other more complicated algorithms, such as the Fourier coefficient (e.g., Rité 1999). Each spectrum is linearized in log λ, has the continuum removed by a low-order polynomial, and is end-masked with a cosine bell function prior to the cross-correlation analysis. Following Baggley (1996) and Wegner et al. (1999) the measurements of redshift and velocity dispersion are carried out in two steps. A first estimate of the redshift and FWHM is obtained using the whole observed spectrum. Next, using the first redshift estimate an improved measurement of the redshift and of the FWHM of the cross-correlation peak is obtained by restricting the wavelength range. For each galaxy-template combination the FWHM of the correlation peak is calculated using the spectral region with rest wavelength 4770–5770 Å. This FWHM is then calibrated by convolving each standard star's spectrum with a series of Gaussian broadening functions to construct a curve relating the cross-correlation peak FWHM with the input σ value.

Internal errors in the measurement of the velocity dispersions arise from systematic errors associated with the template-galaxy mismatches and the statistical errors due to the noise properties of the spectra. The errors in the σ's were estimated by calibrating the Tonry & Davis (1979) R value, the height of the true peak to the average peak in the cross-correlation, using simulated spectra with different noise values and indicates that our error estimates depend on S/N and the velocity dispersion. The velocity dispersion dependence arises because at low σ one is limited by the instrumental resolution, while at high σ the absorption lines broaden leaving only a small contrast relative to the continuum. Both effects tend to increase the amplitude of the error.

The internally defined error is normalized on a run by run basis from the ratio of the standard deviation of repeated exposures of the same galaxy, observed in the same run and with approximately the same S/N, to the internal error estimate. All internal errors for that run are multiplied by this factor. Figure 4 shows our final estimates of the fractional error $\delta\sigma/\sigma$ as a function of σ the velocity dispersion (*left*) and the $\delta\sigma/\sigma$ distribution (*right*), for all the observed galaxies. As can be seen on the left side for $\log\sigma \gtrsim 2.2$ the errors are essentially constant but then rise at the low-σ end, which comprises less than 10% of the sample.

3.2. *Aperture Corrections*

The velocity dispersions were corrected by applying an aperture correction to the observed velocity dispersion. This accounts for the dependence of the measured velocity dispersions on: (1) observational parameters, such as the seeing and the size and shape of the spectrograph slit; (2) the galaxy's distance, since a fixed slit size projects to different physical scales on galaxies with distances; (3) the intrinsic velocity and luminosity profiles of the galaxy. Expressions for the aperture correction were obtained empirically by Davies et al. (1987) and by Jørgensen et al. (1995b) using kinematical models. Here we adopt the latter's metric aperture correction:

$$\log\left(\frac{\sigma_{\rm cor}}{\sigma_{\rm obs}}\right) = 0.038\log\left[\left(\frac{r_{\rm ap}}{r_{\rm norm}}\right)\left(\frac{cz}{cz_0}\right)\right], \qquad (1)$$

where $\sigma_{\rm obs}$ is the value of the velocity dispersion observed through an equivalent circular aperture of $r_{\rm ap}$, which for a

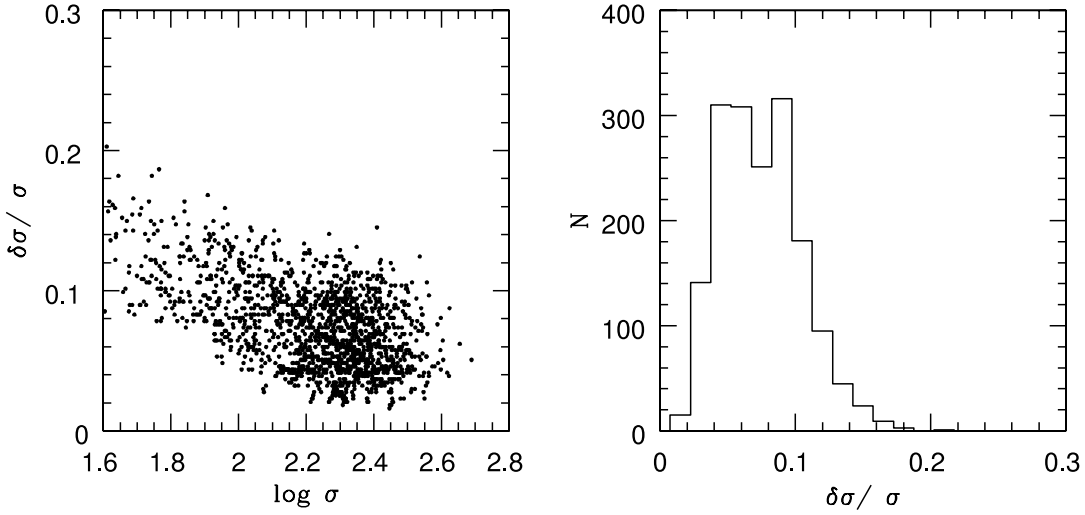

FIG. 4.—*Left*: Fractional error of the velocity dispersion $\delta\sigma/\sigma$ as function of σ for all the ENEAR observed spectra. *Right*: Distribution of the velocity dispersion fractional errors $\delta\sigma/\sigma$.

rectangular slit is $r_{ap} = 1.025(wl/\pi)^{1/2}$ in arcseconds, w and l being the width and length of the slit and σ_{cor} is the corrected value normalized to a circular aperture of radius $r_{norm} = 0.595\ h^{-1}$ kpc, cz is the redshift of the galaxy, and cz_0 is a reference redshift taken to be that of Coma ($cz_0 = 7010$ km s^{-1}). The standard aperture corresponds to 1.″7 at the Coma distance.

3.3. *Line Strengths*

We have also measured the Mg_2 index and scaled it to the Lick system for all the available spectra. This line index is an indicator of metallicity and star formation rate (e.g., Bernardi et al. 1998; Colless et al. 1999). The Mg_2 index is given in magnitudes and measures the depression of the spectral intensity due to the combined broad Mg H feature and the Mg b triplet and is defined as

$$\mathrm{Mg}_2 = -2.5 \log \frac{\int_{\lambda_1}^{\lambda_2} S(\lambda)/C(\lambda) d\lambda}{\Delta\lambda}\ , \qquad (2)$$

where $\Delta\lambda = \lambda_2 - \lambda_1 = 42.5$ Å is the width of the Mg_2 bandpass (5154.1–5196.6 Å), $S(\lambda)$ is the object spectrum and $C(\lambda)$ is a pseudocontinuum. Following González (1993) and Worthey et al. (1994) the pseudocontinuum is estimated by a linear interpolation between the midpoints of the side bands (4895.1–4957.6 and 5301.1–5366.1 Å) where the average flux is computed within these two side bands.

Most of our spectra lacked spectrophotometric flux calibrations and had resolutions higher than the Lick system, so we adopted the following procedure to measure the Mg_2 line index. First, all spectra were degraded in resolution by smoothing with a Gaussian filter with a width chosen to match the spectral resolution of the Lick/IDS (8.6 Å). Second, the detector response was accounted for on a run-by-run basis. For each run a low-order polynomial (1–3) was fitted to the spectra of galaxies in common with Faber et al. (1989) over a wavelength range of about 500 Å. The order of the fit was chosen so that, after dividing the observed spectra by this polynomial and measuring the Mg_2 index, a good agreement with Faber et al. (1989) was obtained. This polynomial was then retained for all spectra in the run, leaving the zero point free. Figure 5 shows the resulting differences between our measured Mg_2 line indices and those of Faber et al. (1989). The order of the polynomial depends on the resolution. For our low-resolution spectra a linear fit worked well, while a polynomial of order greater than 3 was required in the case of high-resolution spectra.

In the Mg_2 indices we find no significant zero-point shift and a relatively small scatter of 0.015 mag. We have also measured the Mg_2 index directly, ignoring possible variations in the response function for runs with available Lick standards. In these cases the line index is computed for the stars, the resulting value is then corrected to the Lick values and the same correction applied to the galaxies. The two methods lead to consistent results, with a scatter of about 0.014 mag, comparable to those obtained from the comparison with galaxies measured in the Lick system by Faber et al. (1989).

The Mg_2 line strength errors were estimated using simulated spectra. For each run all high-S/N stellar templates were used to generate a set of spectra of different S/N and velocity dispersions. This was done by adding Poisson noise and convolving with Gaussians of varying width to simulate galaxies with different velocity dispersions. For each template a total of about 1000 simulated spectra were generated in 50 km s^{-1} intervals of velocity dispersion and S/N ranging from 10 to 60. For each template σ and S/N the rms value of the measurement of the Mg_2 index, following the same procedure adopted above, was computed. Thus, an error grid was generated for each template. The error in the Mg_2 measurement for an object was taken to be the largest value at the appropriate value of σ and S/N.

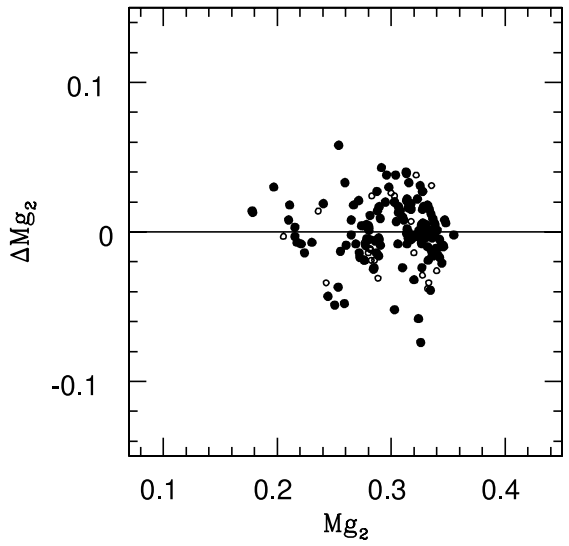

FIG. 5.—Comparisons of the Mg_2 measurements obtained by Faber et al. (1989) (Lick system) with the values derived on the ENEAR spectra observed at low resolution (*open circles*) and on ENEAR spectra observed at high resolution (*filled circles*).

Figure 6 shows resulting distribution of the estimated errors δMg_2 in the measurement of the Mg_2 line index for all of our galaxies found using the procedure described above. We find that the median error is 0.013 ± 0.002 mag, comparable to the values obtained by other authors (e.g.,

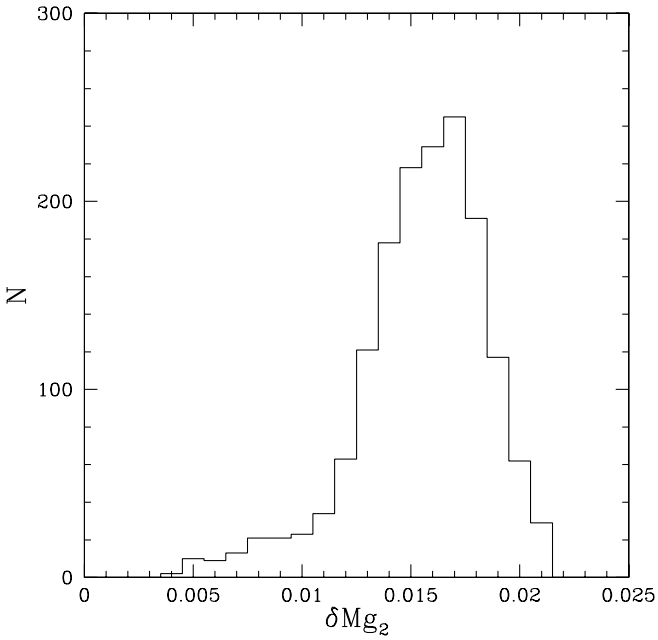

FIG. 6.—Distribution of the errors associated to the ENEAR measurements of the Mg_2 line index using the simulated spectra described in the text.

Jørgensen, Franx, & Kjærgaard 1995a, 1995b; Colless et al. 1999).

Our final Mg_2 line indices are corrected for aperture effects and for the broadening of the line due to the velocity dispersion of the galaxies, which underestimates the value of the index for high-σ galaxies (e.g., González 1993). Following Jørgensen et al. (1995b), we have adopted an aperture correction for the Mg_2 index that is similar to the one used for the velocity dispersion:

$$\mathrm{Mg}_2^{\mathrm{cor}} - \mathrm{Mg}_2^{\mathrm{obs}} = 0.038 \log\left[\left(\frac{r_{\mathrm{ap}}}{r_{\mathrm{norm}}}\right)\left(\frac{cz}{cz_0}\right)\right] \qquad (3)$$

The σ broadening correction used here was derived as follows. The spectra of standard stars available in a run were first convolved with Gaussians of different dispersions. Next the ratio between the value of the index as measured in the original unconvolved spectra to that measured on the convolved spectra was determined as function of the velocity dispersion. A smooth curve was fitted to the ratios obtained for different templates. The correction for a galaxy of a given σ was obtained from this fit. All runs have shown a similar correction of $\sim$0.001 mag at $\sigma = 100$ km s^{-1}, which increases approximately linearly to $\sim$0.004 mag at $\sigma = 400$ km s^{-1}.

4. INTERNAL AND EXTERNAL COMPARISONS

In order to make our spectroscopic measurements from different runs internally consistent, we find that only relative zero-point shifts are necessary. Therefore, measurements obtained in different observing runs are brought onto a common system by applying these zero-point corrections. This procedure takes into account the number of overlaps available at each site and for each setup. It optimizes the number of overlaps in the comparison to improve the statistics in the determination of the offset required to bring them into a common system. The high-resolution ESO data (setup 4 in Table 2) are taken as the reference. These data were chosen as the fiducial system because they have the highest resolution, comprise the largest number of spectra in our sample, and have the greatest number of galaxies with repeated observations in common with other instrumental setups.

To determine the "fiducial" system, we corrected our spectroscopic parameters using the mean difference Δx_i of the measurements of run i with all the other runs $j \neq$ i for galaxies in run j in common with those in i. This offset is computed with variance weighting using the estimated errors in each measurement:

$$\Delta x_i = \epsilon_i^2 \sum_{j \neq i} \sum_{k \epsilon i,j} \frac{x_{i,k} - x_{j,k}}{\Delta x_{i,k}^2 + \Delta x_{j,k}^2} \ . \qquad (4)$$

Here k runs over the galaxies in common between runs i and j, and $x_{i,k}$ corresponds to the measurement of either log σ or Mg_2 for galaxy k in run i and ϵ_i is the standard error in the mean, estimated by:

$$\epsilon_i = \left(\sum_{j \neq i} \sum_{k \epsilon i,j} \frac{1}{\Delta x_{i,k}^2 + \Delta x_{j,k}^2} \right)^{-1/2} . \qquad (5)$$

We determine the most significant offset by finding the run with the maximum value of $\Delta x_i / \epsilon_i$ and iterate toward a common zero point by subtracting this offset from the measurements of run i. We halt the process when the most significant offset was $\Delta x_i / \epsilon_i < 2$. About four iterations were required for redshift, velocity dispersion, and the Mg_2 index parameters. These corrections are relatively small amounting to less than 25 km s^{-1}, with a scatter of 40 km s^{-1} for redshift, $\lesssim$0.025 dex with a scatter $\lesssim$0.060 dex for log σ, and $\lesssim$0.015 mag with a scatter of $\sim$0.020 mag for Mg_2. After defining the fiducial system, we compare aperture corrected values, whenever necessary, obtained using different setups at ESO.

The relatively large number of overlapping observations provide the necessary information to derive suitable statistical corrections for all runs at different sites. When making this comparison, we used the convention of performing the differences between "older/newer" measurements. For instance, we compared a measurement taken in the first ESO-651 run with all the subsequent ESO runs. We then compared the second run (ESO-652) measurements with all later runs (ESO-653, 654, etc., but not ESO-651) and so on. The measurements obtained from MDM and CASLEO spectra were corrected as follows: for runs with a significant number of galaxies in common with our reference system the measured values were directly compared with this system, while for other runs, where the number of galaxies in common is small, the comparison was made using calibrated measurements for that telescope and setup.

The offsets derived from the comparison of all other runs not used in the definition of the fiducial system are small and therefore consistent with those offsets found in defining the reference system. This indicates the high degree of homogeneity of the data. Only one CASLEO run, which contributes the least to the overall sample, required a large offset correction, $\Delta \log \sigma = 0.064$ dex.

The final results of the uniformization are presented in Figure 7, which shows the comparison between the ESO measurements of log σ (*left*) and Mg_2 line index (*right*), with those obtained from ESO, MDM, and CASLEO spectra (*top to bottom*). The results are summarized in Table 3, which gives: in columns (1)–(2) the sites; in column (3) the number of repeated measurements N_m in the same or in different runs; in columns (4) and (5) the mean offset and its error of the differences of the calibrated log σ and (6) and (7) of the Mg_2 measurements. These results show that the corrections lead to an internally consistent system with only a small ($\lesssim$1%) residual offset in the velocity dispersion. The last two rows report the internal comparisons for MDM and CASLEO.

After bringing all measurements to a consistent system, multiple measurements of the same galaxy are combined weighting by their individual errors as described in the next section. These final values are then compared with those of previous studies in the literature, as presented in Figures 4 and 5 of Bernardi et al. (2002a). As shown in that paper, we find an overall residual difference between ENEAR measurements and those in the literature of -0.002 ± 0.004 dex and a scatter of 0.051 in log (σ). For Mg_2 we find an offset of 0.003 ± 0.002 mag and a scatter of 0.018 mag. These observed scatters are consistent with an error per galaxy of about 8% in velocity dispersion and 0.01 mag in Mg_2. Note, however, that most of the available data in the literature is limited to values $\gtrsim$100 km s^{-1} and $Mg_2 \gtrsim 0.18$ mag. As seen in the internal estimates above, we expect increasing measurement errors for these smaller quantities as one approaches the resolution limit.

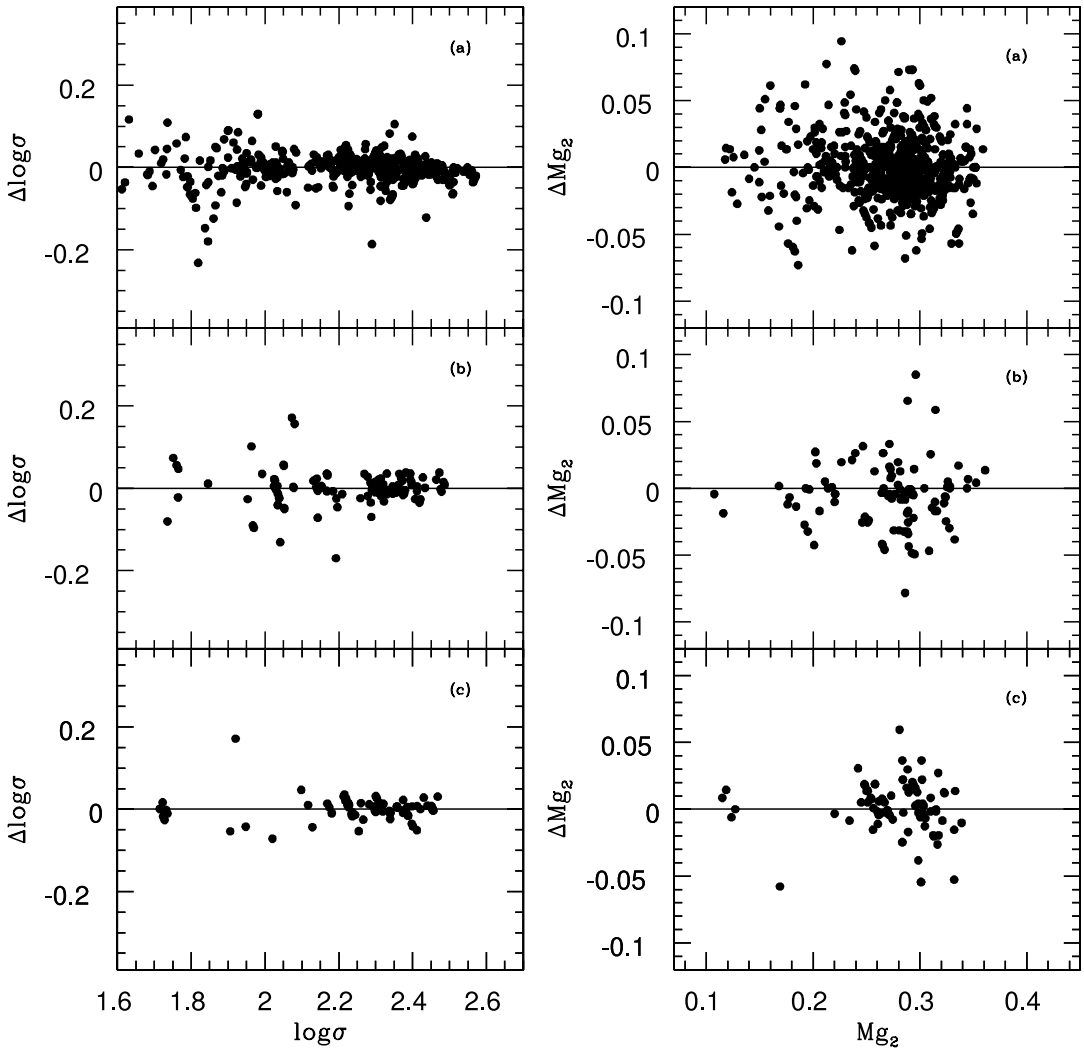

FIG. 7.—Internal consistency of the derived velocity dispersion (*left*) and Mg_2 line index (*right*). Internal comparisons between measurements obtained at ESO (setups 1 to 4) and measurements obtained at: ESO (*a*), MDM (setups 5 to 10, *b*), and CASLEO (setup 11, *c*).

5. THE SPECTROSCOPIC CATALOG

The final value of each of the spectroscopic parameters for a galaxy with multiple observations is given by the error-weighted mean of the individual measurements. The error for these galaxies is computed by adding in quadrature the error associated to the mean with the rms scatter of the repeated measurements. Whenever necessary, values that differ by more than 3 times the rms from the mean were removed to avoid biasing the results due to a few outliers. For small values of σ and Mg_2 only the measurements obtained at high resolution are used.

Table 4 lists the final fully corrected and, if more than one observation is available, combined spectroscopic data for 1178 galaxies from the ENEAR observations; no literature data are used.[14] The photometric portion of the ENEAR

[14] In comparing data in Table 4 with those in common with Bernardi et al. (2002b), some differences occur as a result of two causes. First, Bernardi et al. include literature data in the averages and in this paper only ENEAR data are included. Second, Table 4 is a later compilation of ENEAR spectroscopic data. Some additional observations were added and the homogenization of the runs to a common system were recomputed; differences were usually small or unchanged.

TABLE 3
INTERNAL COMPARISONS

Site 1	Site 2	N_m	$\langle\Delta\log\sigma\rangle$	rms/$\sqrt{2}$	$\langle\Delta Mg_2\rangle$	rms/$\sqrt{2}$
ESO	ESO	745	0.004 ± 0.002	0.038	-0.001 ± 0.001	0.018
ESO	MDM	110	-0.006 ± 0.006	0.038	-0.001 ± 0.002	0.020
ESO	CASLEO	89	0.008 ± 0.006	0.035	0.003 ± 0.003	0.019
MDM	MDM	77	0.002 ± 0.005	0.029	0.001 ± 0.003	0.019
CASLEO	CASLEO	13	0.011 ± 0.013	0.033	-0.001 ± 0.006	0.016

TABLE 4

THE SPECTROSCOPIC ENEAR CATALOG

Name (1)	α (J2000.0) (2)	δ (J2000.0) (3)	T (4)	m_B (mag) (5)	$N_{\rm obs}$ (6)	$cz_{\rm hel}$(km s^{-1}) (7)	$\epsilon_{cz_{\rm hel}}$(km s^{-1}) (8)	log σ(km s^{-1}) (9)	$\epsilon_{\log\sigma}$(km s^{-1}) (10)	$N_{\rm Mg_2}$ (11)	Mg$_2$ (12)	$\epsilon_{\rm Mg_2}$ 13)	Notes (14)	Lit. (15)
ESO 409G012	00 04 42.2	−30 29 00	−5	14.23	1	8044	63	2.386	0.040	1	0.242	0.011	1	*
IC 1529	00 05 13.3	−11 30 12	−2	14.50	3	6726	25	2.258	0.022	3	0.254	0.012	1	
NGC 7832.....	00 06 28.4	−03 42 58	−3	13.50	2	6202	19	2.351	0.032	2	0.285	0.013	1	
UGC 00061	00 07 23.8	+47 02 26	−2	14.30	2	5354	52	2.312	0.031	2	0.303	0.011	1	
NGC 0043.....	00 13 00.8	+30 54 55	−2	13.90	2	4846	20	2.298	0.042	2	0.323	0.010	1	
UGC 00130.....	00 13 56.9	+30 52 58	−7	14.20	1	4792	30	2.146	0.042	1	0.273	0.012	1	
NGC 0050.....	00 14 44.5	−07 20 38	−3	12.50	1	5468	22	2.422	0.026	0	0.000	0.000	1	
NGC 0063.....	00 17 45.6	+11 27 01	−5	12.60	2	1167	26	1.875	0.060	2	0.111	0.024	4, 3	
NGC 0068.....	00 18 18.7	+30 04 17	−3	14.05	1	5790	29	2.414	0.032	1	0.304	0.009	1	
NGC 0078A.....	00 20 25.8	+00 49 34	−2	14.50	1	5454	26	2.398	0.033	1	0.308	0.009	1	
NGC 0108.....	00 25 59.0	+29 12 41	−2	13.30	2	4776	25	2.197	0.032	2	0.264	0.013	1	
NGC 0113.....	00 26 54.5	−02 30 03	−3	14.00	1	4372	25	2.161	0.036	0	0.000	0.000	1	
NGC 0125.....	00 28 50.1	+02 50 17	−2	13.83	1	5263	24	2.105	0.062	1	0.212	0.008	1	
NGC0128	00 29 15.0	+02 51 51	−2	12.92	1	4210	21	2.383	0.029	0	0.000	0.000	1	

NOTES.—Table 4 is presented in its entirety in the electronic edition of the Astronomical Journal. A portion is shown here for guidance regarding its form and content. Units of right ascension are hours, minutes, and seconds, and units of declination are degrees, arcminutes, and arcseconds. Col. (14): (1) no problems; (2) star along the slit; (3) emission lines; (4) low-S/N measurements; (5) low-velocity dispersion on the limit of the resolution; (6) old data (Reticon); (7) peculiar spectrum: e.g., broad lines (supernova?), absorption lines too weak or undetectable.

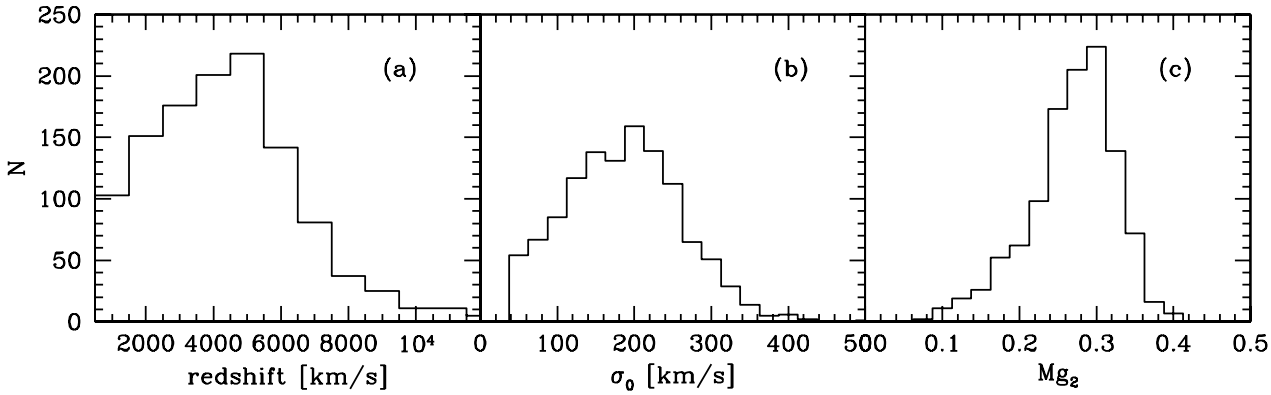

FIG. 8.—Distribution of (*a*) redshift, (*b*) velocity dispersion, and (*c*) Mg_2 line strength for galaxies in the ENEAR sample

survey is given in Alonso et al. (2003); it should be noted however that not all objects have both kinds of data. The table shows: in column (1) the galaxy standard name; in columns (2) and (3) the (J2000.0) equatorial coordinates; in column (4) the morphological parameter T (see Paper I); in column (5) the photographic magnitude m_B; in column (6) $N_{\rm obs}$, the number of spectra used for redshift and σ; in columns (7) and (8) the heliocentric redshift and error; in columns (9) and (10) the velocity dispersion and error; in column (11) $N_{\rm Mg_2}$ the number of spectra used to determine the Mg_2 line index; in columns (12) and (13) the Mg_2 line index and its error; in column (14) notes; and column (15) denotes whenever the galaxy has data form the literature. Here we present only the first few entries of the table, which can be retrieved in its entirety from the electronic version of this journal.

The redshift, velocity dispersion and Mg_2 line index distributions for the 1178 galaxies listed in Table 4 are shown in Figure 8. The sharp break seen in the redshift distribution at $cz = 7000$ km s^{-1} reflects the redshift cutoff of the ENEARm sample. Galaxies beyond this redshift are in clusters or are fainter than $m_B = 14.5$. Also note that a significant number of galaxies ($\gtrsim$100) have been measured at the low-σ ($\lesssim$100 km s^{-1}) and small line index end ($\lesssim$0.20) where the number of such galaxies with measured values in the literature is remarkably small.

The individual measurements used to construct Table 4 are given in Table 5, for which we also present the first few entries and the entire table can be obtained from the electronic version of this journal. These measurements include the run corrections described above and the table contains: column (1) is the galaxy standard name; columns (2) and (3) give the (J2000.0) equatorial coordinates; column (4) is the morphological type (T); column (5) is the magnitude m_B; column (6) is the run number from Table 1; columns (7) and (9) contain the heliocentric redshift and error; columns (9) and (10) are log σ and error; and columns (11) and (12) are the measured Mg_2 line index and error.

TABLE 5
INDIVIDUAL ENEAR SPECTROSCOPIC MEASUREMENTS

Name (1)	α (J2000.0) (2)	δ (J2000.0) (3)	T (4)	m_B (mag) (5)	Run (6)	$cz_{\rm hel}$ (km s^{-1}) (7)	$\epsilon_{cz_{\rm hel}}$ (km s^{-1}) (8)	log σ (km s^{-1}) (9)	$\epsilon_{\log\sigma}$ (km s^{-1}) (10)	Mg_2 (mag) (11)	ϵ_{Mg_2} (mag) (12)
ESO409G012	00 04 42.2	−30 29 00	−5	14.23	660	8044	63	2.386	0.040	0.242	0.012
IC1529	00 05 13.3	−11 30 12	−2	14.50	653	6735	30	2.251	0.029	0.257	0.011
	...	...	...	...	656	6725	22	2.259	0.018	0.248	0.006
	...	...	...	...	653	6724	23	2.260	0.016	0.270	0.011
NGC7832	00 06 28.4	−03 42 58	−3	13.50	653	6202	22	2.368	0.034	0.276	0.013
	...	...	...	...	653	6203	16	2.343	0.024	0.290	0.009
UGC00061	00 07 23.8	+47 02 26	−2	14.30	508	5362	57	2.311	0.036	0.296	0.013
	...	...	...	...	508	5350	47	2.312	0.024	0.304	0.004
NGC0043	00 13 00.8	+30 54 55	−2	13.90	508	4854	22	2.287	0.051	0.317	0.011
	...	...	...	...	508	4843	16	2.301	0.027	0.325	0.006
UGC00130	00 13 56.9	+30 52 58	−7	14.20	505	4792	30	2.146	0.042	0.273	0.014
NGC0050	00 14 44.5	−07 20 38	−3	12.50	501	5468	22	2.422	0.026	0.000	0.004
NGC0063	00 17 45.6	+11 27 01	−5	12.60	651	1143	20	1.835	0.058	0.088	0.012
	...	...	...	...	667	1180	14	1.896	0.042	0.131	0.011
NGC0068	00 18 18.7	+30 04 17	−3	14.05	503	5790	29	2.414	0.032	0.304	0.010
NGC0078A	00 20 25.8	+00 49 34	−2	14.50	502	5454	26	2.398	0.033	0.308	0.013
NGC0108	00 25 59.0	+29 12 41	−2	13.30	508	4786	25	2.198	0.038	0.261	0.012

NOTES.—Table 5 is presented in its entirety in the electronic edition of the Astronomical Journal. A portion is shown here for guidance regarding its form and content.

6. SUMMARY

We have presented spectroscopic observations for the ENEAR project and described their reduction and quality assessment. There are 1701 spectra of 1178 galaxies, of which ~80% had no previous measurements of redshift, velocity dispersion, and Mg_2 line index. In addition to the velocity dispersions, we have measured the Mg_2 index for 1149 galaxies. About 80% of the observations were conducted with a resolution of $\lesssim 2.5$ Å, which is a factor of 2 better than previous large surveys. The observations span a number of years utilizing different instruments, but repeated observations allow the measurements to be brought into a common system that is internally consistent and compares well with published data. From the comparison with external data we confirm our error estimates which are typically of ~8% in σ and 0.01 mag in Mg_2. The errors are nearly constant for $\sigma > 100$ km s^{-1} and $Mg_2 > 0.2$ mag, increasing for smaller values.

Since there is considerable overlap with measurements of velocity dispersion and Mg_2 by other authors (Bernardi et al. 2002a, 2002b), it is possible to derive statistical corrections that can be applied to these other measurements to produce a uniform catalog of about 2000 early-type galaxies with measured velocity dispersions and 1300 with measured Mg_2 line index. Such a sample is an invaluable database for studies of the properties of the early-type galaxies and their peculiar motions. Our sample is currently one of the largest uniform data sets of spectroscopic measurements of nearby early-type galaxies.

G. W. acknowledges support from the following over the course of this project: Dartmouth College, the Alexander von Humboldt Stiftung for a year's stay at the Ruhr Universität in Bochum, and ESO for supporting trips to Garching. M. B. thanks the Sternwarte München, the Technische Universität München, ESO Studentship program, and MPA Garching for their financial support during different phases of this research. C. N. A. W. acknowledges partial support from CNPq grants 301364/86-9, 453488/96-0, and NSF AST 95-29028 and NSF AST 00-71198. M. V. A. would like to acknowledge the hospitality of the Harvard-Smithsonian Center for Astrophysics, the ESO visitor program, and ON. We wish to thank the CNPq-NSF bilateral program (M. V. A., L. N. d. C.), acknowledge a research fellowship from CNPq (P. S. S. P.), and thank CLAF (M. V. A., P. S. S. P., and M. A. G. M.) for financial support to the project. M. V. A. also acknowledges financial support from the SECYT and CONICET (Argentina). Nearly all of the southern observations were carried out using the 1.54 m ESO telescope thanks to an agreement between ESO and the Observatório Nacional.

REFERENCES

Aaronson, M., Huchra, J., Mould, J., Schechter, P. L., & Tully, R. B. 1982, ApJ, 258, 64
Alonso, M. V., Bernardi, M., da Costa, L. N., Wegner, G., Wilmer, C. N. A., Pellegrini, P. S., & Maia, M. A. G. 2003, AJ, 125, 2307
Baggley, G. 1996, Ph.D. thesis, Oxford Univ.
Bernardi, M., Alonso, M. V., da Costa, L. N., Willmer, C. N. A., Wegner, G., Pellegrini, P. S., Rité, C., & Maia, M. A. G. 2002a, AJ, 123, 2159
———. 2002b, AJ, 123, 2990
Bernardi, M., Renzini, A., da Costa, L. N., Wegner, G., Alonso, M. V., Pellegrini, P. S., Rité, C. N. A., & Willmer, C. N. A. 1998, ApJ, 508, L143
Bertschinger, E., Dekel, A., Faber, S. M., Dressler, A., & Burstein, D. 1990, ApJ, 364, 370
Borgani, S., Bernardi, M., da Costa, L. N., Wegner, G., Alonso, M. V., Willmer, C. N. A., Pellegrini, P. S., & Maia, M. A. G. 2000, ApJ, 537, L1
Burstein, D., Davies, R. L., Dressler, A., Faber, S. M., Stone, R. P. S., Lynden-Bell, D., Terlevich, R., & Wegner, G. 1987, ApJS, 64, 601
Burstein, D., Faber, S. M., & Dressler, A. 1990, ApJ, 354, 18
Colless, M., Burstein, D., Davies, R. L., McMahan, R. K., Jr., Saglia, R. P., & Wegner, G. 1999, MNRAS, 303, 813
Colless, M., Saglia, R. P., Burstein, D., Davies, R. L., McMahan, R. K., & Wegner, G. 2001, MNRAS, 321, 277
Courteau, S., Faber, S. M., Dressler, A., & Willick, J. A. 1993, ApJ, 412, L51
Courteau, S., Willick, J. A., Strauss, M. A., Schlegel, D., & Postman, M. 2000, ApJ, 544, 636
da Costa, L. N., Bernardi, M., Alonso, M. V., Wegner, G., Willmer, C. N. A., Pellegrini, P. S., Maia, M. A. G., & Zaroubi, S. 2000b, ApJ, 537, L81
da Costa, L. N., Bernardi, M., Alonso, M. V., Wegner, G., Willmer, C. N. A., Pellegrini, P. S., Rité, C., & Maia, M. A. G. 2000a, AJ, 120, 95 (Paper I)
da Costa, L. N., Freudling, W., Wegner, G., Giovanelli, R., Haynes, M. P., & Salzer, J. J. 1996, ApJ, 468, L5
da Costa, L. N., Nusser, A., Freudling, W., Wegner, G., Giovanelli, R., Haynes, M. P., Salzer, J. J., & Wegner, G. 1998a, MNRAS, 299, 425
da Costa, L. N., Pellegrini, P. S., Nunes, M. A., Willmer, C., Chincarini, G., & Cowan, J. 1986, AJ, 91, 6
da Costa, L. N., et al. 1998b, AJ, 116, 1
da Costa, L. N., Willmer, C., Pellegrini, P. S., & Chincarini, G. 1987, AJ, 93, 1338
Davies, R. L., Burstein, D., Dressler, A., Faber, S. M., Lynden-Bell, D., Terlevich, R., & Wegner, G. 1987, ApJS, 64, 581
Dekel, A. 2000, in ASP Conf. Ser. 201, Cosmic Flows: Towards an Understanding of Large-Scale Structure, ed. S. Courteau, M. A. Strauss, & J. A. Willick (San Francisco: ASP), 420
Dressler, A., Lynden-Bell, D., Burstein, D., Davies, R. L., Faber, S. M., Terlevich, R., & Wegner, G. 1987, ApJ, 313, 42
Faber, S. M., Wegner, G., Burstein, D., Davies, R. L., Dressler, A., Lynden-Bell, D., & Terlevich, R. J. 1989, ApJS, 69, 763
Feldman, H. A., et al. 2003, preprint (astro-ph/0305078)
Giovanelli, R., & Haynes, M. P., Freudling, W., da Costa, L. N., Salzer, J. J., & Wegner, G. 1998, ApJ, 505, L91
González, J. 1993, Ph.D. thesis, Univ. California, Santa Cruz
Haynes, M. P., Giovanelli, R., Chamaraux, P., da Costa, L. N., Freudling, W., Salzer, J. J., & Wegner, G. 1999b, AJ, 117, 2039
Haynes, M. P., Giovanelli, R., Salzer, J. J., Wegner, G., Freudling, W., da Costa, L. N., Herter, T., & Vogt, N. P. 1999a, AJ, 117, 1668
Hudson, M. J., Smith, R. J., Lucey, J. R., Schlegel, D. J., & Davies, R. L. 1999, ApJ, 512, L79
Jørgensen, I., Franx, M., & Kjærgaard, P. 1995a, MNRAS, 273, 1097
———. 1995b, MNRAS, 276, 1341
Lauberts, A., & Valentijn, E. A. 1989, The Surface Photometry Catalogue of the ESO-Uppsala Galaxies (Garching: ESO)
Lauer, T. R., & Postman, M. 1994, ApJ, 425, 418
Lynden-Bell, D., Faber, S. M., Burstein, D., Davies, R. L., Dressler, A., Terlevich, R., & Wegner, G. 1988, ApJ, 326, 19
Mathewson, D. S., & Ford, V. L. 1996, ApJS, 107, 97
Mathewson, D. S., Ford, V. L., & Buchhorn, M. 1992, ApJS, 81, 413
Müller, K., Freudling, W., Watkins, R., & Wegner, G. 1998, ApJ, 507, L105
Müller, K. R., Wegner, G., Raychaudhury, S., & Freudling, W. 1999, A&AS, 140, 327
Nusser, A., da Costa, L. N., Branchini, E., Bernardi, M., Alonso, M. V., Wegner, G., Willmer, C. N. A., & Pellegrini, P. S. 2001, MNRAS, 320, L21
Nusser, A., & Davis, M. 1994, ApJ, 421, L1
Rité, C. 1999, Ph.D. thesis, CNPq/Observatório Nacional
Riess, A. G. 2000, in ASP Conf. Ser. 201, Cosmic Flows: Towards and Understanding of Large-Scale Structure, ed. S. Courteau, M. A. Strauss, & J. A. Willick (San Francisco: ASP), 80
Rubin, V. C., Roberts, M. S., Thonnard, N., & Ford, W. K., Jr. 1976, AJ, 81, 719
Strauss, M. A., & Willick, J. A. 1995, Phys. Rep., 261, 271
Tammann, G. A., & Sandage, A. 1985, ApJ, 294, 81
Tonry, J. L., Blakeslee, J. P., Ajhar, E. A., & Dressler, A. 2000, ApJ, 530, 625
Tonry, J. L., & Davis, M. 1979, AJ, 84, 1511
———. 1981, ApJ, 246, 666
Wegner, G., Colless, M., Baggley, G., Davies, R. L., Bertschinger, E., Burstein, D., McMahan, R. K., & Saglia, R. P. 1996, ApJS, 106, 1

Wegner, G., Colless, M., Saglia, R. P., McMahan, R. K., Davies, R. L., Burstein, D., & Baggley, G. 1999, MNRAS, 305, 259
Willick, J. A. 1990, ApJ, 351, L5
Willick, J. A., Courteau, S., Faber, S. M., Burstein, D., Dekel, A., & Strauss, M. A. 1997, ApJS, 109, 333
Willick, J. A., & Strauss, M. A. 1998, ApJ, 507, 64
Worthey, G., Faber, S. M., González, J. J., & Burstein, D. 1994, ApJS, 94, 687
Woudt, P. A., Kraan-Korteweg, R. C., & Fairall, A. P. 1999, A&A, 352, 39
Zaroubi, S., Bernardi, M., da Costa, L. N., Hoffman, Y., Alonso, V., Wegner, G., Willmer, C. N. A., & Pellegrini, P. S. 2001, MNRAS, 326, 375
Zaroubi, S., Branchini, E., Hoffman, Y., & da Costa, N. 2002, MNRAS, 336, 1234
Zaroubi, S., Zehavi, I., Dekel, A., Hoffman, Y., & Kolatt, T. 1997, ApJ, 486, 21

Note added in proof.—Two galaxies are misidentified in Table 6 of our companion photometric paper (Alonso et al. 2003, AJ, 125, 2307). The correct coordinates of IC 5349 differ slightly and galaxy D54-080 should be D54-079. The correct names and coordinates are given in Tables 4 and 5 of this paper. The first galaxy's name is correct but has the wrong coordinates, and both the name and coordinates of the second one are incorrect.